A Dynamic Model for Nozzle Clog Monitoring in Fused Deposition Modelling

Yedige Tlegenov, Wong Yoke San, Hong Geok Soon
Department of Mechanical Engineering, National University of Singapore,
9 Engineering Drive 1, Singapore 117575, Singapore

Abstract

Purpose – Fused deposition modelling (FDM) is one of the most popular additive manufacturing (AM) processes, and is widely used for prototyping and fabricating low cost customised parts. Current FDM machines have limited techniques to monitor process conditions in order to minimise process errors, such as nozzle clogging. Nozzle clogging is one of the most significant process errors in current FDM machines, and may cause serious consequences such as print failure. This paper presents a physics-based dynamic model suitable for monitoring nozzle clogging in FDM machines.

Design/Methodology/Approach – Liquefier mount of FDM extruder is analysed as a beam excited by a uniform loading distributed over a partial length. Boundary conditions and applied loads for direct type FDM extruder are identified and discussed. Simulation of nozzle clogging was performed by using nozzles of different diameter from 0.5 mm to 0.2 mm, in step change of 0.1 mm. Sets of experiments were carried out by measuring vibrations of the liquefier block mount during FDM extrusion.

Findings – The mount of a liquefier block in FDM extruder can be used to place a vibration sensor in order to monitor process errors such as nozzle clogging. Liquefier block mount's transverse vibration amplitudes increase non-linearly when nozzle starts to block.

Practical implications – The proposed model can be effectively used for monitoring nozzle clogging in FDM machines, as it is based on the physics relating the FDM process parameters and the nozzle blockage.

Originality/value – The novelty of this paper is the unique method of modelling the FDM process dynamics that can be used for monitoring nozzle clogging.

Keywords 3D printing, Fused deposition modelling, Dynamic model, Nozzle clogging, Process monitoring.

Paper type Research paper

1. Introduction

The development of additive manufacturing (AM) processes will probably lead to technological improvements in various engineering areas, including bioengineering (Murphy & Atala, 2014), (Geng, et al., 2005), electronics (Lewis & Ahn, 2015), (Joe Lopes, et al., 2012), and robotics (Tlegenov, et al., 2014), (Telegenov, et al., 2015). One of the most popular AM processes is fused deposition modelling (FDM) (Crump, 1992). Parts manufactured via FDM machine are created as computer-aided design (CAD) files, converted into a format which includes only surface geometry (for example, .stl format), and sent to a FDM machine for 3D printing. During 3D printing, the filament is fed into liquefier, where it melts and extrudes through a nozzle onto a build table via a computer-controlled three-axis stage, by forming a thin cross-section layer of a part. After completion of one layer the table is lowered (or the extruder is moved upwards), and the next cross-sectional layer of a part is formed. This process repeats for all cross sectional layers (or slices), until the part is fully manufactured in three dimensions. The commonly used material for FDM is thermoplastics, such as acrylonitrile butadiene styrene (ABS), polyactic acid (PLA), polycarbonate (PC), polyamide (PA), polystyrene (PS), rubber, and others. FDM is commonly used for prototyping, testing, manufacturing low cost detailed parts and customized manufacturing tools. However, there are number of quality problems of the parts fabricated using FDM, such as geometry deviations (Huang & Singamneni, 2015), (Melenka, et al., 2015), (Weiss, et al., 2015), (Wesley Machado Cunico & de Carvalho, 2013), (Singh, 2014), surface roughness defects (Boschetto, et al., 2013), (Armillotta, 2006), (Rojas Arciniegas & Esterman, 2015), and mechanical strength issues (Ahn, et al., 2002), (Rodríguez, et al., 2003), (Bellini & Güçeri, 2003), (Sun, et al., 2008), (Durgun & Ertan, 2014), (Agarwala, et al., 1996). These and other quality issues of the fabricated parts are resulted from number of FDM process errors. In order to minimize the process errors, there are various guidelines developed for each FDM machine settings, such as extrusion and feed velocity, liquefier and chamber temperature, extrusion and table calibration, etc. However, the FDM process conditions are not monitored online, and may vary during operation, resulting in process errors. Thus, there is a need in analysing the fundamental principles of how the process parameters are related to the process errors for developing effective FDM condition monitoring technique. In addition, FDM condition monitoring may be very significant for increasing the quality of fabricated parts. To sum up, the FDM process is one of the most popular and promising 3D printing technique, but has serious issues with quality problems of parts and print failure. These problems need to be resolved via fundamental process analysis and FDM condition monitoring.

There are several studies reported on condition monitoring of extrusion based layered fabrication processes, which are discussed as follows. To start with, vision-based monitoring in layered manufacturing was reported by Fang et al. (Fang, et al., 1998), (Fang, et al., 2003), where optical image of each layer was examined and compared with the ideal layer morphology using machine vision techniques. Secondly, Rao et al. (Rao, et al., 2015) proposed online condition monitoring in fused filament fabrication (FFF) based on non-parametric Bayesian Dirichlet Process mixture model using multiple sensors, such as thermocouples, accelerometers, an infrared temperature sensor, and video borescope. They experimentally investigated the relationship effect of input parameters (feed/flow rate ratio, layer height, and extruder temperature) on the surface roughness of the fabricated part. Thirdly, Wu et al. (Wu, et al., 2015) presented FDM condition monitoring technique using acoustic emission for identification abnormal states during fabrication process. They experimentally identified three abnormal states of the FDM machine, such as run out of material, semi-blocked extruder, and completely blocked extruder. Although the above mentioned reports investigate layered AM condition monitoring using various sensors such as vision, thermal, acoustic emission and others, it can be noted that these studies have not addressed the fundamental physics of the process, and thus were limited to fully interpret the resulting errors during operation. Fourthly, Bukkapatnam et al. (Bukkapatnam & Clark, 2007) developed physics-based dynamic model of contour crafting (CC) layered manufacturing process. They modelled the CC machine as nonlinear two degrees of freedom lumped mass system which was excited by forces such as filament feeding force, drive mechanism force, backpressure force, and others. Their model captured vibration signals gathered from four accelerometers, which were placed on the extruder head and machine frame. The monitoring system based on this dynamic model identified such process errors as overflow, underflow, fast feed, and slow feed. However, it can be noted that less attention has been paid to the force arising from flow through the nozzle and the boundary conditions. To summarize, researchers reported a number of monitoring techniques for layered manufacturing processes. Several studies have tended to focus on empirical process error detection using multiple sensors, rather than on the physics of that process. Another study was based on physics-based dynamic model and captured vibrations during operation, but did not fully consider one of the main process forces and boundary conditions, and hence were limited in the representation of the full dynamics of the system.

From the above mentioned literature review there are no known studies reported on physics-based dynamic modelling and monitoring of nozzle clogging in FDM, and the current

study attempts to fill this research gap. Nozzle clogging is one of the most significant process errors in AM, and may cause several problems such as geometrical misalignments or failure during printing (Kim, et al., 2015). There are three main reasons of the nozzle clogging phenomenon, namely, presence of external particles on the filament, filament burn inside of the nozzle, and the absence of place for extrusion (Bellini, 2002). Currently nozzle clogging problems cannot be handled automatically on FDM machines (Heller, 2015), and only the FDM machine operator can identify it visually, after which it is required to manually stop the operation, clean the nozzle, and reprint the whole part from the scratch.

The objectives of the present research are to: a) propose a physics-based theoretical model of the FDM process dynamics that represents fundamental relationships between process parameters and nozzle clogging phenomenon; (b) simulate the blocked nozzle based on the developed model; and (c) compare these findings with the actual experiments. The novelty of the present research is the unique method of modelling the FDM process dynamics with respect to the nozzle clogging phenomenon. In particular, the extruder's bar mount is analysed as a pinned-pinned beam excited by a uniform loading distributed over a partial length. The model includes a crucial process parameter, which is the flow-through-nozzle force, which was not considered in previous studies (Bukkapatnam & Clark, 2007), (Rao, et al., 2015), (Wu, et al., 2015). In addition, the boundary conditions of the system are identified and discussed, such that the model can be easily adjusted for other types of FDM extruders. The location of the accelerometer placement on the FDM machine was carefully chosen and relies on the proposed physics-based model, unlike in the earlier studies (Rao, et al., 2015), (Bukkapatnam & Clark, 2007) where the sensors were placed on the surface of the extruder block assembly.

The rest of the paper is organized as follows. Section 2 presents the theoretical process model of nozzle clogging in FDM, simulation and experimental methods. Section 3 illustrates the theoretical and experimental results. Section 4 discusses the significance which is followed by the conclusion.

2. Methods

The methodology includes theoretical modelling of the FDM process with respect to nozzle clogging phenomenon, simulation of the nozzle clogging based on the developed theoretical model, and experimental verification, discussed in the following section.

2.1. Dynamic process modelling

Consider the FDM extruder shown in Figure 1. Generally it consists of a stepper motor, drive gear, drive block, bar mount, heated liquefier, and nozzle. The heated liquefier is connected to the bar mount by a thermal tube and supported by a nut at the top. The working principle of FDM extruder is as follows. First, a stepper motor powers the drive gear, which feeds the filament into the heated liquefier. Next, the solid filament acts as a piston and pushes the molten filament into the liquefier, which results in the extrusion of the melted filament through a nozzle. The dynamic process modelling methodology includes several main parts, namely, problem statement, boundary conditions, beam analysis, and identification of applied loads.

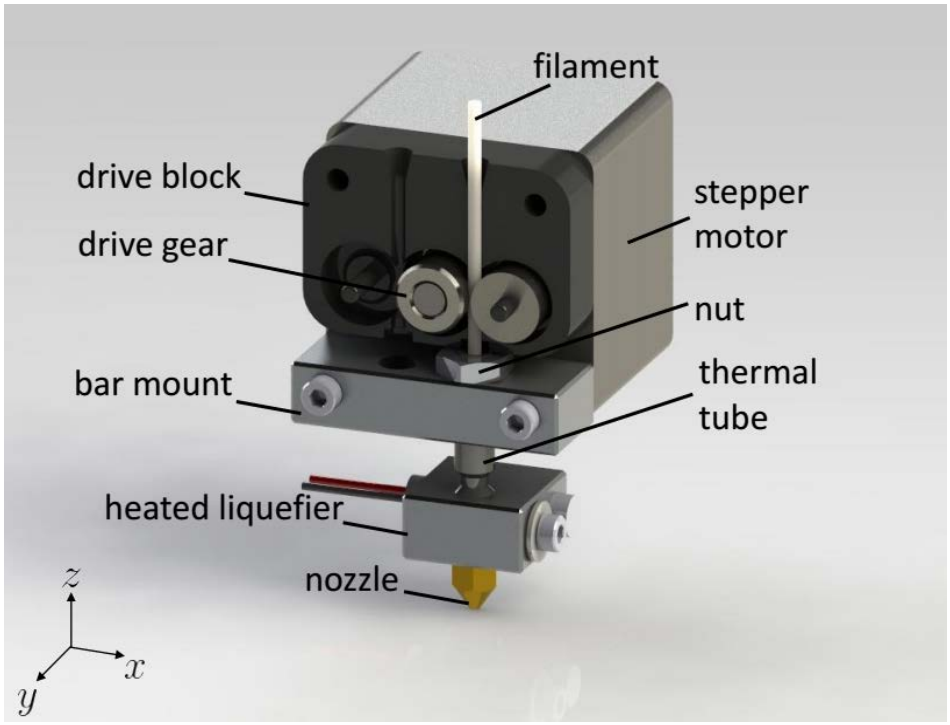

Figure 1. 3D layout of FDM extruder

2.1.1. Problem statement, boundary conditions, and beam analysis

As can be seen from Figure 1, the liquefier and nozzle are connected via a thermal tube, which is fixed to the bar mount by a nut at the top. Consequently, any disturbances affecting the liquefier and nozzle along the z-axis are also affecting the thermal tube in the longitudinal direction. Thus, the longitudinal disturbances of the thermal tube directly affect the nut, and the nut distributes the applied forces uniformly over its contact area with the bar mount. Therefore it can be noted that any forces affecting the liquefier and nozzle along the z-axis directly affect the bar mount in the same direction.

Based on the above mentioned, the bar mount is modelled as a beam with known geometry and material parameters. In addition, the excitations affecting the extruder along the z-axis are

This is a pre-print of an article Yedige Tlegenov, Yoke San Wong, Geok Soon Hong, (2017) "A dynamic model for nozzle clog monitoring in fused deposition modelling", Rapid Prototyping Journal, Vol. 23 Issue: 2, pp.391-400. The final authenticated version is available online at: https://doi.org/10.1108/RPJ-04-2016-0054

modelled to be distributed over a contact area of the nut with the bar mount. As a result, the FDM extruder's bar mount can be modelled as a pinned-pinned beam, as shown in Figure 2. The partial length of the beam is excited by a uniform loading, which depend on the size of the nut.

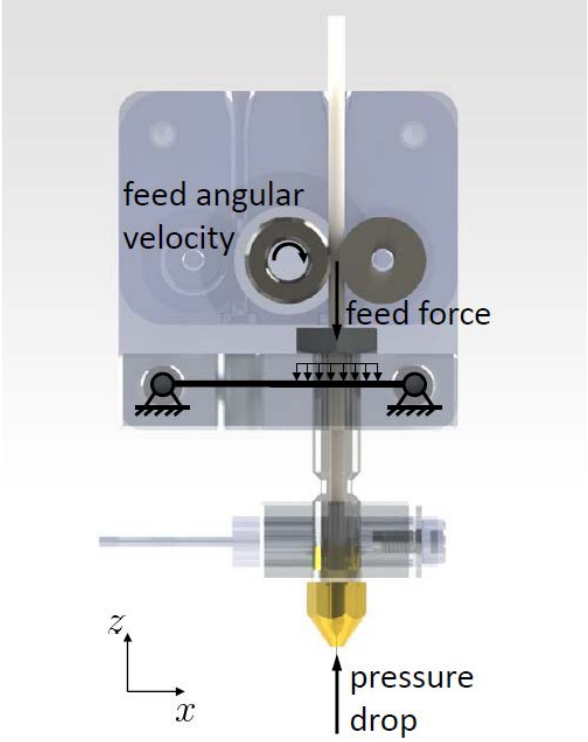

Figure 2. 2D layout of FDM extruder and projected beam model

Thus, the FDM extruder analysed in this study is a direct extruder type, where the extruder motor is directly above the liquefier. Apart from the direct extruder type, there are several other types of FDM extruders available on commercial market. For example, the Bowden extruder type is widely used in FDM printers, where the extruder motor is placed relatively far away from the filament entry to the liquefier. However, it can be noted that the dynamic modelling of the Bowden extruder can be performed in a similar manner as direct extruder, by adjusting filament feeding force. Furthermore, there are plenty of heater block (also referred as hot end) types available for FDM extruders, with various range of materials and sizes. Nevertheless nearly all of them are mounted in a similar way, i.e. liquefier and nozzle are connected to the mount, which can be modelled as a beam. Thus, it can be noted that the modelling of other types of heater blocks can be done in the same way with proper adjustments of the boundary conditions. To sum up, the FDM extruder model introduced in current study can be treated as novel dynamic model that can be applied near to all structural types of FDM extruders.

This is a pre-print of an article Yedige Tlegenov, Yoke San Wong, Geok Soon Hong, (2017) "A dynamic model for nozzle clog monitoring in fused deposition modelling", Rapid Prototyping Journal, Vol. 23 Issue: 2, pp.391-400. The final authenticated version is available online at: https://doi.org/10.1108/RPJ-04-2016-0054

The forced lateral response of a pinned-pinned beam excited by a uniform loading over a partial length of the beam is shown in Figure 3.

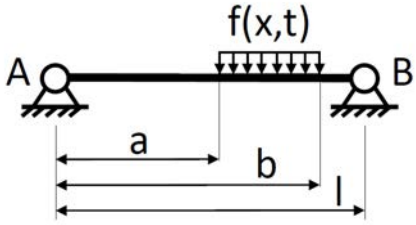

Figure 3. Pinned-pinned elastic beam subjected to a partially distributed uniform loading

The beam is assumed to have uniform cross section and material properties. The governing equation of the model can be written as (Barnoski, 1965)

$$m(x)\ddot{z}(x,t) + c(x)\dot{z}(x,t) + D(x)z(x,t) = f(x,t) \tag{1}$$

where $m(x)$ is beam mass per unit length, $c(x)$ is beam viscous damping coefficient per unit length, $z(x,t)$ is lateral displacement of beam, $D(x)$ is spatial differential operator, $f(x,t)$ is force function acting on the structure (will be discussed in section 2.1.2). The modal solution for the lateral displacement $z(x,t)$ from (1) can be written as

$$z(x,t) = \sum_j \phi_j(x)q_j(t), \qquad \text{for } j = 1,2,\ldots \tag{2}$$

where $\phi_j(x)$ is jth normal mode of the system, $q_j(t)$ is the generalized coordinate. For the Euler-Bernoulli beam the differential operator can be expressed as

$$D(x) = EI\frac{\partial^4}{\partial x^4} \tag{3}$$

where E is the modulus of elasticity and I is the second moment of area of the beam cross section. Hence, the governing equation (1) for the current problem can be rewritten as (Barnoski, 1965)

$$m(x)\ddot{z}(x,t) + c(x)\dot{z}(x,t) + EI\frac{\partial^4 z(x,t)}{\partial x^4} = f(x,t) \tag{4}$$

In order to solve (4) there is a need to determine the mode shape and generalized coordinate. The detailed calculation in terms of generalized coordinates is provided in Appendix A.

To sum up, the dynamic process modelling of FDM extruder with respect to nozzle clogging is performed by assuming the bar mount as Euler-Bernoulli beam excited by a uniform loading distributed over a partial length. The beam boundary conditions are identified as pinned at both ends, and the modal solution for the lateral displacement of the beam can then be appropriately obtained with appropriately defined boundary conditions.

2.1.2. Identification of applied loads

This is a pre-print of an article Yedige Tlegenov, Yoke San Wong, Geok Soon Hong, (2017) "A dynamic model for nozzle clog monitoring in fused deposition modelling", Rapid Prototyping Journal, Vol. 23 Issue: 2, pp.391-400. The final authenticated version is available online at: https://doi.org/10.1108/RPJ-04-2016-0054

The applied loading consists of two main opposite forces, namely, feed force and flow-through-nozzle force. To start with, the feed force acts downwards along the z-axis and depends on filament parameters, stepper motor characteristics and the distance between locations where filament feeds and where the filament enters into liquefier (also referred as unsupported filament length). On the other hand, the flow-through-nozzle force depends mainly on the pressure drop in the liquefier. The vector summation of these two main forces plus the gravity force represents the partially distributed uniform loading acting on a pinned-pinned beam.

Filament feeding force acting along the z-axis is a function of the stepper motor torque and the roller radius. For the system with two feeding rollers the filament feeding force can be derived as (N. Turner, et al., 2014)

$$F_{feed} = \frac{2T_z}{R_{roller}} \tag{12}$$

where T_z is torque of filament feeding motor along z-axis, R_{roller} is radius of the filament feeding roller. However, there exists the upper limit to the torque that the feed roller motor can provide, because when compression of filament reaches a critical limit, the feedstock filament can buckle. The critical force that can be placed on the filament can be obtained from an Euler buckling analysis for pin-ended boundary condition (Venkataraman, et al., 2000)

$$F_{feedCR} = \frac{\pi^2 E_{fil} I_{fil}}{L_{ulf}^2} \tag{13}$$

where F_{feedCR} is critical feeding force, E_{fil} is Young's modulus of the filament, I_{fil} area moment of inertia of cross section of the filament, L_{ulf} is unsupported length of the filament.

The flow-through-nozzle force depends on the pressure drop in the nozzle, where the solid filament is melted and pushed through the liquefier. The pressure drop (isothermal) of the nozzle can be derived as the sum of all pressure drops in three zones of the nozzle, as shown in Figure 4 (Michaeli, 2003), (Bellini, et al., 2004), (N. Turner, et al., 2014):

$$\Delta p_1 = 2L_1 \left(\frac{v}{\chi}\right)^{\frac{1}{q}} \cdot \left(\frac{q+3}{R_1^{q+1}}\right)^{\frac{1}{q}} \tag{14}$$

$$\Delta p_2 = \frac{2q}{3\tan(\alpha/2)} \left(\frac{1}{R_1^{3/q}} + \frac{1}{R_2^{3/q}}\right) \cdot \left(\frac{vR_2^2(q+3)}{\chi}\right)^{\frac{1}{q}} \tag{15}$$

$$\Delta p_3 = 2L_3 \left(\frac{v}{\chi}\right)^{\frac{1}{q}} \cdot \left(\frac{(q+3)R_1^2}{R_2^{q+1}}\right)^{\frac{1}{q}} \tag{16}$$

where Δp is pressure drop, v is flow mean velocity, χ is flow consistency index, q is flow behaviour index, R_1, R_2 are nozzle radius values at the entry and at the outer regions respectively, L_1, L_3 are nozzle length values in the zone 1 and 3 respectively, α is an inside angle of the nozzle.

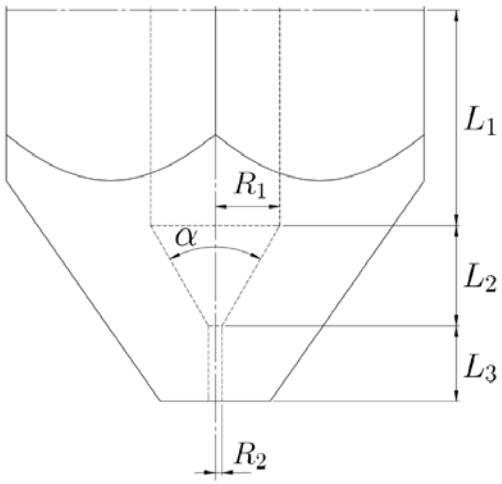

Figure 4. Nozzle layout with three zones

The total pressure drop is then calculate as (Michaeli, 2003), (Bellini, et al., 2004), (N. Turner, et al., 2014)

$$\Delta p = \Delta p_1 + \Delta p_2 + \Delta p_3 \tag{17}$$

The Arrhenius Law is taken into consideration for the temperature dependence (Bellini, et al., 2004), (N. Turner, et al., 2014)

$$H(T) = e^{\beta\left(\frac{1}{T}-\frac{1}{T_0}\right)} \tag{18}$$

where T is operation temperature and $T_0$is absolute temperature. The temperature dependent pressure drop can be calculated by (Bellini, et al., 2004), (N. Turner, et al., 2014)

$$\Delta p_T = \Delta p \cdot e^{\beta\left(\frac{1}{T}-\frac{1}{T_0}\right)} \tag{19}$$

Thus the flow-through-nozzle force can now be derived as (Bellini, et al., 2004), (N. Turner, et al., 2014)

$$F_{flow} = \Delta p_T \cdot A_{fil} \tag{20}$$

where A_{fil} is cross sectional area of the filament.

After calculation of the feeding force and flow-through-nozzle force the total force acting on a beam can be obtained from

$$\bar{W} = \bar{F}_{feed} + \bar{F}_{flow} + \bar{G}_{extr} \tag{21}$$

where W is a total uniform force acting on a simply supported beam over a partial length, G_{extr} is gravity force of extruder system.

2.2. Numerical simulation of nozzle clogging

Numerical simulation of the nozzle clogging was performed by calculating the natural frequency of the system and derivation the of the Fourier amplitude spectrum of acceleration when the nozzle is blocked. The process parameters used in the current study are based on MakerBot Stepstruder MK7 commercial extruder (MakerBot Replicator 2, 2016), (MakerBot Stepstruder, 2016), (Melenka, et al., 2015) and listed in Table I. The numerical simulation involves the following steps:

- The clogging phenomenon was simulated by setting the initial nozzle diameter to 0.5 mm, and the clogged nozzle diameters at 0.4, 0.3, and 0.2 mm.
- The natural frequency of the system was obtained from equation (9) using parameters listed in Table I.
- The Fourier amplitude spectrum of acceleration was calculated from equation (10) using characteristics presented in Table I.

After investigating the frequency response to a load distributed over partial length of a beam, the data were saved and imported to MATLAB software for building the resultant graphs.

Table I. Process parameters

Parameter	Description/Value
Bar mount material	Aluminium
Bar mount size, length x width x height	30 x 13 x 16 mm
Stepper motor torque	0.285 Nm
Drive gear diameter	10.8 mm
Filament type	ABS plastic
Filament diameter	1.75 mm
Extrusion temperature	230 Celsius
Extrusion speed	50 mm/sec
Internal angle of nozzle	110 degrees
Nozzle diameters	0.5 mm - 0.2 mm
Chamber temperature	32 Celsius
Young's modulus of Aluminium	70 GPa
Young's modulus of ABS plastic	1.5 GPa
ABS melt viscosity	155 Pa·s
Flow consistency index	633 $Pa \cdot s^n$
Flow behaviour index	0.6

2.3. Experimental setup

The experimental setup based on MakerBot Stepstruder MK7 commercial extruder (MakerBot Replicator 2, 2016), (MakerBot Stepstruder, 2016), (Melenka, et al., 2015) to verify the proposed dynamic model is shown in Figures 5 and 6.

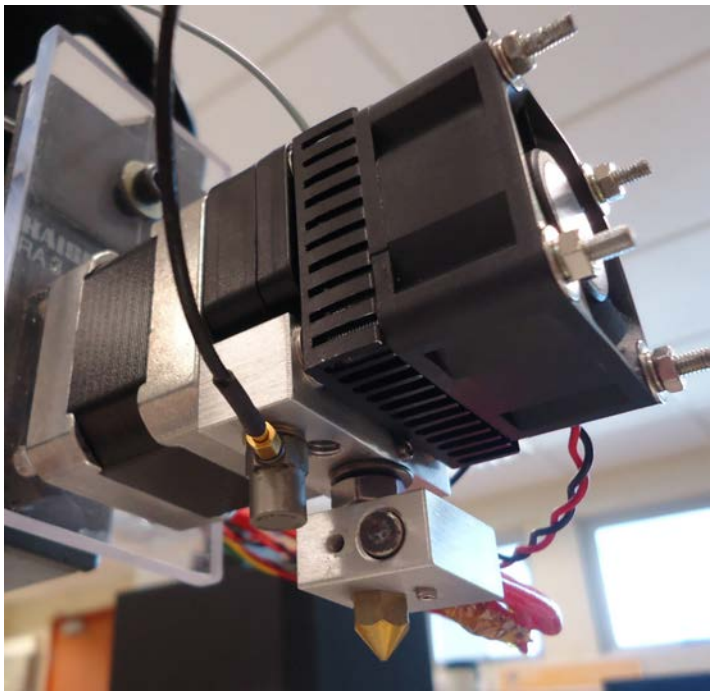

Figure 5. FDM extruder with accelerometer attached to the bar mount

The test parameters were set as follows:

- Extruder: MakerBot MK7 Stepstruder (MakerBot Replicator 2, 2016), (MakerBot Stepstruder, 2016), (Melenka, et al., 2015).
- Controller board: RepRap Arduino Mega Pololu Shield (RAMPS) 1.4 (RepRap Arduino Mega Pololu Shield, 2016) and an Arduino Mega 2560 board (Arduino, 2016).
- Accelerometer: Bruel and Kjaer 4393 Piezoelectric charge accelerometer (Brüel & Kjær, 2016) with mass of 2.4 gram, and sensitivity of 3.1 pC/g. The accelerometer was placed on the bottom side of the bar mount.
- Charge amplifier: Bruel and Kjaer Charge Amplifier type 2635 (Brüel & Kjær Sound & Vibration Measurement A/S, 2016) with output unit set as acceleration in m/s^2.
- Signal analyser: Hewlett Packard 35670a Dynamic Signal Analyser (Keysight Technologies , 2016).
- Nozzles: 0.5 mm, 0.4 mm, 0.3 mm, and 0.2 mm in diameter made of brass.

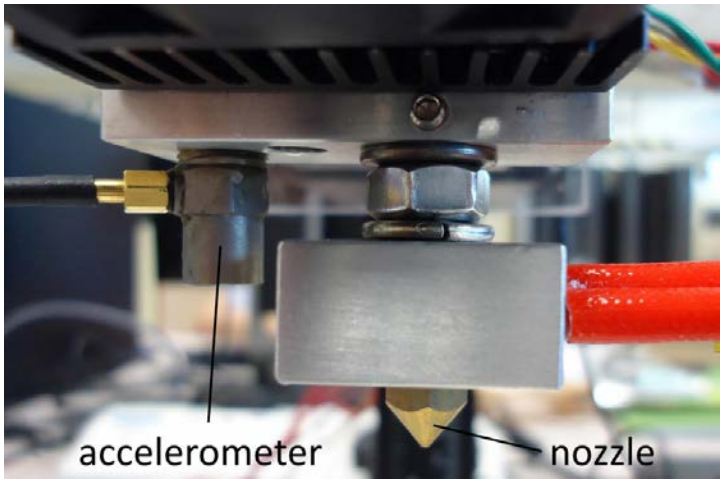

Figure 6. Placement of the accelerometer

The experimental process parameters are listed in Table I. The FDM extruder's clogging phenomenon was simulated during experiment by reducing the diameter of the nozzle. In particular, the initial nozzle diameter used was 0.5 mm, and then subsequent nozzles have diameter of 0.4, 0.3, and 0.2 mm, and the vibrations of the bar mount were measured during filament extrusion for each nozzle size. The vibration signals were analysed in time and frequency domain.

3. Results

Natural Frequency. The simulated and experimental results of the natural frequency and acceleration amplitudes are shown in Table II. The theoretical natural frequency was calculated to be 198 Hz and found experimentally to be 200 Hz. The theoretical and experimental Fourier amplitude spectra of acceleration about the natural frequency were obtained for each nozzle size (from 0.5 mm to 0.2 mm), and the differences were found to be in the range of 10%. Hence, the theoretical model is relatively accurate for determining the natural frequency and the corresponding Fourier acceleration amplitude of the bar mount transverse vibration during filament extrusion.

Table II. Comparison of simulated and experimental results

Results		Simulated		Experimental	
Natural frequency, Hz		198		200	
		value	percentage	value	percentage
Natural frequency amplitudes of acceleration for each nozzle diameter	0.5 mm	0.6990	100%	0.7776	100%
	0.4 mm	0.9114	130.386%	1.0128	130.246%
	0.3 mm	1.1035	157.868%	1.2261	157.677%
	0.2 mm	1.6141	230.915%	1.7934	230.632%

This is a pre-print of an article Yedige Tlegenov, Yoke San Wong, Geok Soon Hong, (2017) "A dynamic model for nozzle clog monitoring in fused deposition modelling", Rapid Prototyping Journal, Vol. 23 Issue: 2, pp.391-400. The final authenticated version is available online at: https://doi.org/10.1108/RPJ-04-2016-0054

Frequency Spectrum. The simulated and experimental Fourier acceleration amplitude spectra for each nozzle size are presented in Figures 7-10. As can be seen from Table II and Figures 6-9, the Fourier amplitude spectrum of acceleration sharply increases with the decrease in nozzle diameter. In particular, for the decrease in nozzle diameter from 0.5 mm to 0.2 mm the amplitude of acceleration near the natural frequency value increases from 0.6990 to 1.6141 during simulation, and from 0.7776 to 1.7934 during experiments, or 230.915% and 230.632% respectively. Thus, it can be noted that the theoretical predictions on the relative increase in bar mount's transverse vibrations when the nozzle becomes clogged are essentially accurate.

Amplitude of Natural Frequency. The simulated and experimental peaks of the acceleration amplitudes at around the natural frequency value are shown in Figures 7-11. Figure 11 show the comparison between theoretical and experimental peaks obtained against the four different nozzle diameters. There were five data sets of experimental vibration signals collected for each nozzle size. As can be seen, both theoretical and experimental results of acceleration amplitudes increase non-linearly with decrease of the nozzle diameter. Therefore, the theoretical prediction that the vibration increase is non-linear during nozzle clogging is likely to be correct. Hence, the results show that the proposed theoretical model adequately represents the nozzle clogging phenomenon in FDM as confirmed by the high correlation with the experimental natural frequency, relative change in the natural frequency amplitude with nozzle diameter, and trend of the vibration change.

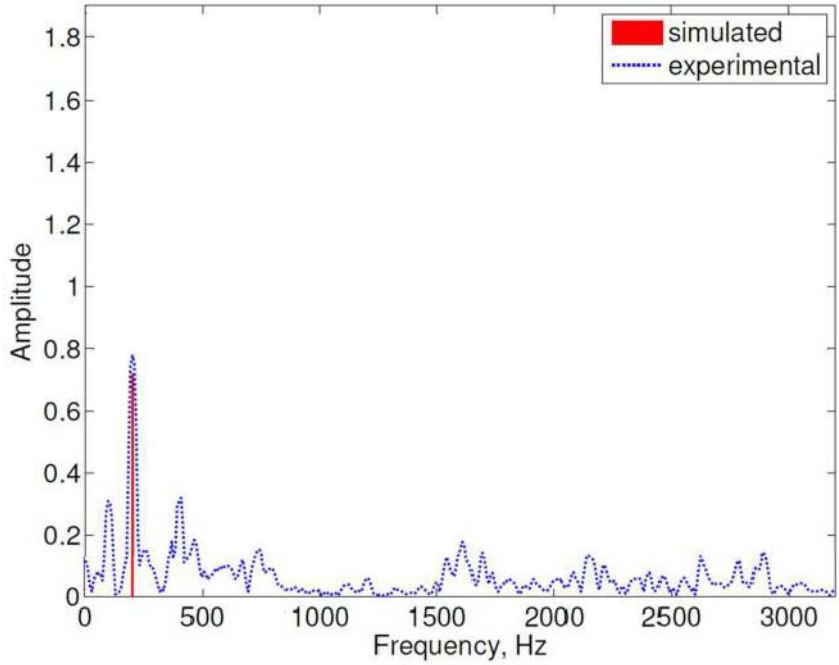

Figure 7. Simulated and experimental values of acceleration amplitudes, 0.5 mm nozzle

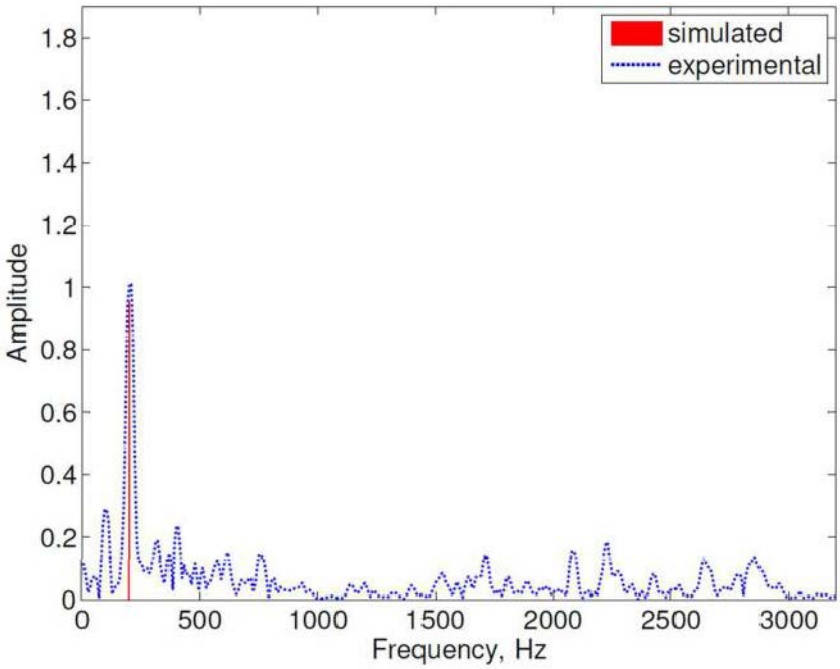

Figure 8. Simulated and experimental values of acceleration amplitudes, 0.4 mm nozzle

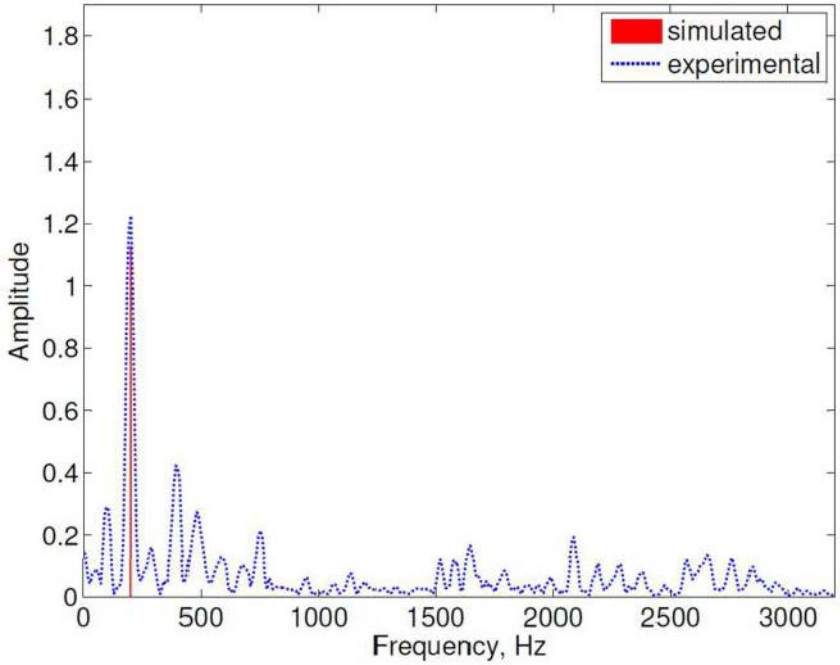

Figure 9. Simulated and experimental values of acceleration amplitudes, 0.3 mm nozzle

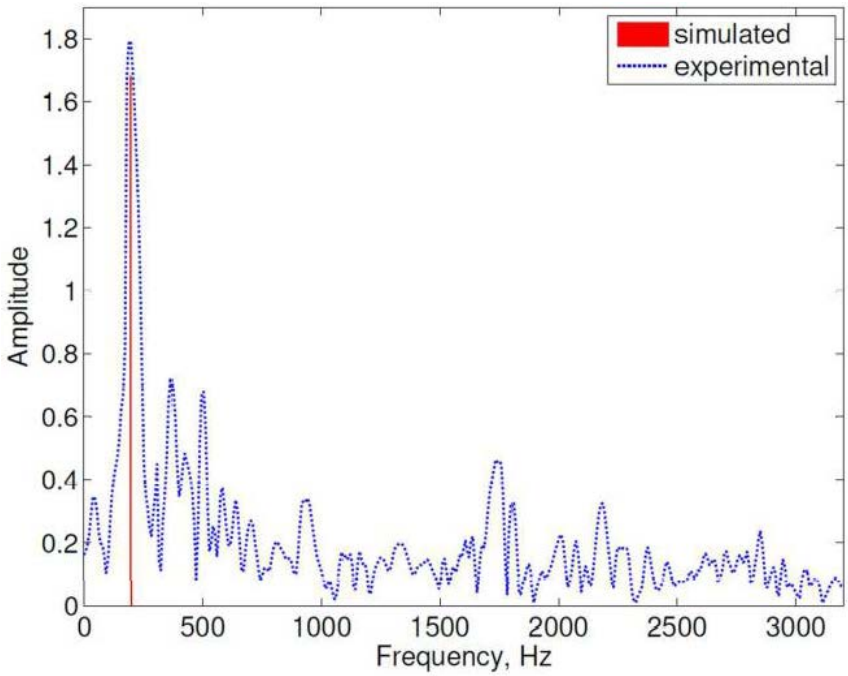

Figure 10. Simulated and experimental values of acceleration amplitudes, 0.2 mm nozzle

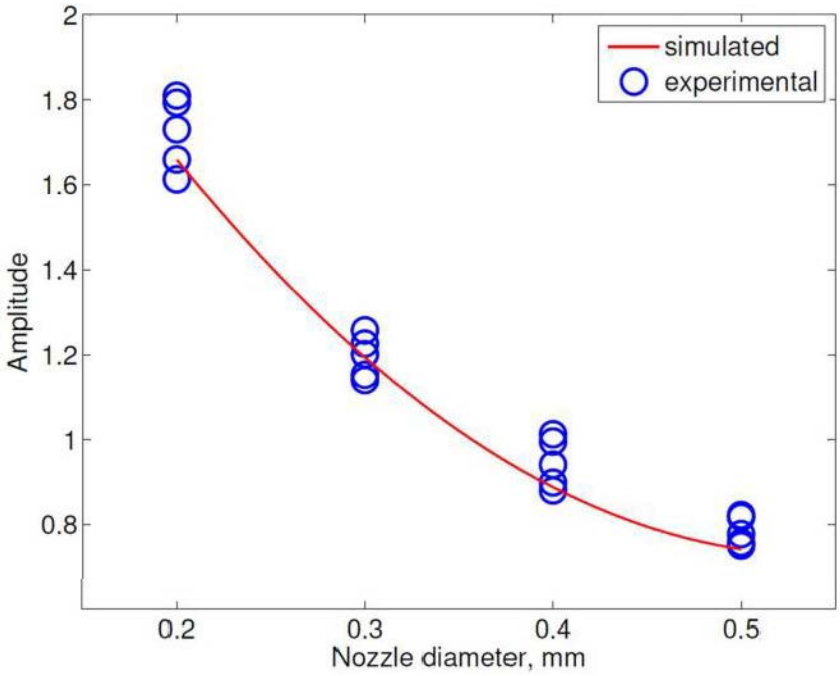

Figure 11. Simulated and experimental values of acceleration amplitudes at natural frequency vs nozzle diameter

4. Discussion

The objective of the current study is to propose physics-based theoretical model of the FDM process dynamics that can predict nozzle clogging phenomenon. In order to achieve this, the extruder's bar mount was analysed as a pinned-pinned beam excited by a uniform loading distributed over a partial length.

There are several findings from theoretical and experimental results, which showed that the proposed model can relatively accurately predict the nozzle clogging phenomenon in FDM machine. First, the calculated natural frequency of the modelled system was very close to the values obtained from the conducted experiments. Second, the theoretical acceleration amplitudes were comparatively near to the values gathered from vibration sensor during the experiment. Third, the proposed model claimed that the FDM extruder's bar mount transverse vibration amplitudes increase with the decrease in nozzle diameter (i.e. nozzle clogging), which was verified with the set of experiments. Fourth, the theoretical model calculations of bar mount transverse vibrations showed non-linear trend during simulated clogging, which was very close to the trend of experimental results. Hence, the proposed dynamic model is relatively adequate for prediction of nozzle blockage in FDM machine.

All of these findings can be significant for monitoring nozzle clogging in FDM machines, as they are based on the fundamental relationships between FDM process parameters and the nozzle blockage. It can be noted that present findings are in contrast to the studies reported by Fang et al. (Fang, et al., 1998), (Fang, et al., 2003), Rao et al. (Rao, et al., 2015), Wu et al. (Wu, et al., 2015) on layer based AM condition monitoring using various sensors such as vision, thermal, acoustic emission and others, which have not addressed the fundamental physics of the process, and thus were limited to fully interpret the resulting errors during operation. Furthermore, findings of the current study are relatively close to the one proposed earlier by Bukkapatnam et al. (Bukkapatnam & Clark, 2007) which was based on dynamic model of FDM machine and captured vibrations during prototyping, but it can be noted that less attention has been paid to the flow-through-nozzle force and the boundary conditions. Another important aspect of the present paper can be clear interpretation of the vibration sensor placement (on the liquefier block mount of FDM extruder), which is in contrast to the previous studies reported on layer based AM condition monitoring (Rao, et al., 2015), (Wu, et al., 2015), (Bukkapatnam & Clark, 2007) where placement of the sensors was not fully addressed.

There are several limitations of the current study. Firstly, theoretical calculation of the forces affecting the bar mount may slightly differ from the real values. This due to the fact that proposed theoretical model includes such process parameters as radius of the filament or liquefier temperature. The radius of the filament and the liquefier temperature mostly vary during operation, and depend on a number of factors, such as filament quality, built environment, heater controller, and others. Secondly, the masses of the wires that are connected

to the heater block were not included in the current study, and thus the theoretical acceleration amplitude results were slightly lower than the experimental values.

Future research may include usage of the proposed model for real time monitoring of nozzle clogging during actual 3D printing using FDM machine using different process parameters and filament materials.

5. Conclusion

Nozzle clogging is one of the most significant process errors in current FDM machines, and may cause serious consequences such as print failure. This paper proposed physics based dynamic model for monitoring nozzle clogging in FDM machines. Moreover, the proposed theoretical model was used to simulate the clogged nozzle during 3D printing, and the results were verified by the set of experiments. Considering this, the following conclusions and recommendations can be suggested.

- The mount of a liquefier block in FDM extruder can be used to place a vibration sensor in order to monitor process errors such as nozzle clogging.
- Depending on the type of the mount, the boundary conditions need to be set appropriately. For example, the bar mount of a direct extruder considered in present study can be modelled as a pinned-pinned beam excited by a uniform loading distributed over a partial length.
- Flow-through-nozzle force is one of the most important parameters to consider for monitoring nozzle clogging. This is due to the fact that flow-through-nozzle force depend on the radius of the nozzle, which decreases when the nozzle becomes clogged.
- The decrease in nozzle radius (can be considered as clogging) increases flow-through-nozzle force, which affects the liquefier block and its mount to the FDM extruder.
- Disturbances on the liquefier block causes its mount to vibrate in transverse direction, which can be tracked via vibration sensors.
- Theoretical and experimental results obtained in present paper show that the transverse acceleration amplitudes of the liquefier block mount increase non-linearly when the nozzle becomes clogged.

In conclusion, the findings of present study can be one step towards developing monitoring nozzle clogging in FDM machines, as they are based on the fundamental relationships between FDM process parameters and the nozzle blockage.

This is a pre-print of an article Yedige Tlegenov, Yoke San Wong, Geok Soon Hong, (2017) "A dynamic model for nozzle clog monitoring in fused deposition modelling", Rapid Prototyping Journal, Vol. 23 Issue: 2, pp.391-400. The final authenticated version is available online at: https://doi.org/10.1108/RPJ-04-2016-0054

References

Murphy, S. V. & Atala, A., 2014. 3d bioprinting of tissues and organs. *Nature biotechnology,* 32(8), pp. 773-785.

Geng, L. et al., 2005. Direct writing of chitosan scaffolds using a robotic system. *Rapid Prototyping Journal,* 11(2), pp. 90-97.

Lewis, J. A. & Ahn, B. Y., 2015. Device fabrication: Three-dimensional printed electronics. *Nature,* 518(7537), pp. 42-43.

Joe Lopes, A., MacDonald, E. & Wicker, R. B., 2012. Integrating stereolithography and direct print technologies for 3D structural electronics fabrication. *Rapid Prototyping Journal,* 18(2), pp. 129-143.

Tlegenov, Y., Telegenov, K. & Shintemirov, A., 2014. *An open-source 3D printed underactuated robotic gripper.* Senigallia, Italy, IEEE, pp. 1-6.

Telegenov, K., Tlegenov, Y. & Shintemirov, A., 2015. A Low-Cost Open-Source 3-D-Printed Three-Finger Gripper Platform for Research and Educational Purposes. *Access, IEEE,* Volume 3, pp. 638-647.

Crump, S. S., 1992. *Apparatus and method for creating three-dimensional objects.* United States of America, Patent No. 5,121,329.

Huang, B. & Singamneni, S. B., 2015. Curved Layer Adaptive Slicing (CLAS) for fused deposition modelling. *Rapid Prototyping Journal,* 21(4), pp. 354-367.

Wesley Machado Cunico, M. & de Carvalho, J., 2013. Optimization of positioning system of FDM machine design using analytical approach. *Rapid Prototyping Journal,* 19(3), pp. 144-152.

Singh, R., 2014. Process capability analysis of fused deposition modelling for plastic components. *Rapid Prototyping Journal,* 20(1), pp. 69-76.

Boschetto, A., Giordano, V. & Veniali, F., 2013. 3D roughness profile model in fused deposition modelling. *Rapid Prototyping Journal,* 19(4), pp. 240-252.

Armillotta, A., 2006. Assessment of surface quality on textured FDM prototypes. *Rapid Prototyping Journal,* 12(1), pp. 35-41.

Rojas Arciniegas, A. J. & Esterman, M., 2015. Characterization and modeling of surface defects in EP3D printing. *Rapid Prototyping Journal,* 21(4), pp. 402-411.

Ahn, S.-H.et al., 2002. Anisotropic material properties of fused deposition modeling ABS. *Rapid Prototyping Journal,* 8(4), pp. 248-257.

Rodríguez, J. F., Thomas, J. P. & Renaud, J. E., 2003. Mechanical behavior of acrylonitrile butadiene styrene fused deposition materials modeling. *Rapid Prototyping Journal,* 9(4), pp. 219-230.

Sun, Q., Rizvi, G., Bellehumeur, C. & Gu, P., 2008. Effect of processing conditions on the bonding quality of FDM polymer filaments. *Rapid Prototyping Journal,* 14(2), pp. 72-80.

Durgun, I. & Ertan, R., 2014. Experimental investigation of FDM process for improvement of mechanical properties and production cost. *Rapid Prototyping Journal,* 20(3), pp. 228-235.

Bellini, A. & Güçeri, S., 2003. Mechanical characterization of parts fabricated using fused deposition modeling. *Rapid Prototyping Journal,* 9(4), pp. 252-264.

Agarwala, M. K. et al., 1996. Structural quality of parts processed by fused deposition. *Rapid Prototyping Journal,* 2(4), pp. 4-19.

Fang, T., Bakhadyrov, I., Jafari, M. A. & Alpan, G., 1998. *Online detection of defects in layered manufacturing.* s.l., IEEE, pp. 254-259.

Fang, T., Jafari, M. A., Danforth, S. C. & Safari, A., 2003. Signature analysis and defect detection in layered manufacturing of ceramic sensors and actuators. *Machine Vision and Applications,* 15(2), pp. 63-75.

Rao, P. K. et al., 2015. Online real-time quality monitoring in additive manufacturing processes using heterogeneous sensors. *Journal of Manufacturing Science and Engineering,* 137(6), p. 061007.

Wu, H., Wang, Y. & Yu, Z., 2015. In situ monitoring of FDM machine condition via acoustic emission. *The International Journal of Advanced Manufacturing Technology,* pp. 1-13.

Bukkapatnam, S. & Clark, B., 2007. Dynamic modeling and monitoring of contour crafting – an extrusion-based layered manufacturing process. *Journal of Manufacturing Science and Engineering,* 129(1), pp. 135-142.

N. Turner, B., Strong, R. & A. Gold, S., 2014. A review of melt extrusion additive manufacturing processes: I. Process design and modeling. *Rapid Prototyping Journal,* 20(3), pp. 192-204.

Venkataraman, N. et al., 2000. Feedstock material property – process relationships in fused deposition of ceramics (FDC). *Rapid Prototyping Journal,* 6(4), pp. 244-253.

Michaeli, W., 2003. *Extrusion dies for plastics and rubber.* s.l.:Carl Hanser Verlag GmbH & Co. KG.

Bellini, A., Guceri, S. & Bertoldi, M., 2004. Liquefier dynamics in fused deposition. *Journal of Manufacturing Science and Engineering,* 126(2), pp. 237-246.

Melenka, G. W., Schofield, J. S., Dawson, M. R. & Carey, J. P., 2015. Evaluation of dimensional accuracy and material properties of the MakerBot 3D desktop printer. *Rapid Prototyping Journal,* 21(5), pp. 618-627.

Barnoski, R. L., 1965. *Response of Elastic Structures to Deterministic and Random Excitation,* Los Angeles: Defense Technical Information Center.

Brüel & Kjær Sound & Vibration Measurement A/S, 2016. *Charge Amplifier - Type 2635.* [Online]
Available at: http://www.bksv.com/Products/transducers/conditioning/charge/2635
[Accessed 29 March 2016].

Brüel & Kjær, 2016. *4393 - Piezoelectric charge accelerometer.* [Online]
Available at:
http://www.bksv.com/Products/transducers/vibration/accelerometers/accelerometers/4393
[Accessed 29 March 2016].

Keysight Technologies , 2016. *35670A FFT Dynamic Signal Analyzer.* [Online]
Available at: http://www.keysight.com/en/pd-1000001335%3Aepsg%3Apro-pn-35670A/fft-dynamic-signal-analyzer-dc-1024-khz?cc=SG&lc=eng
[Accessed 29 March 2016].

MakerBot Replicator 2, 2016. *MakerBot Replicator 2 brochure.* [Online]
Available at:
http://downloads.makerbot.com/replicator2/MakerBot_Replicator2_brochure.pdf
[Accessed 29 March 2016].

MakerBot Stepstruder, 2016. *MakerBot Stepstruder MK7.* [Online]
Available at: http://downloads.makerbot.com/support/pdf/Thing-O-Matic/Docs/Stepstruder%20MK7%20Assembly.pdf
[Accessed 29 March 2016].

RepRap Arduino Mega Pololu Shield, 2016. *RAMPS 1.4.* [Online]
Available at: http://reprap.org/wiki/RAMPS_1.4
[Accessed 29 March 2016].

Arduino, 2016. *Arduino MEGA 2560.* [Online]
Available at: https://www.arduino.cc/en/Main/ArduinoBoardMega2560
[Accessed 29 March 2016].

Bellini, A., 2002. *Fused deposition modeling: a comprehensive experimental, analytical and computational study of material behavior, fabrication process and equipment design.* Drexel University: PhD Thesis.

Heller, B. P., 2015. *Effects of nozzle geometry and extrudate swell on fiber orientation in Fused Deposition Modeling nozzle flow.* Baylor University: MSc Thesis.

Weiss, B., Storti, D. W. & Ganter, M. A., 2015. Low-cost closed-loop control of a 3D printer gantry. *Rapid Prototyping Journal,* 21(5), pp. 482-490.

Kim, C. et al., 2015. *A study to detect a material deposition status in fused deposition modeling technology.* s.l., IEEE, pp. 779-783.

Appendix A

The governing equation in terms of generalized coordinated can be written as (Barnoski, 1965)

$$\bar{M}_j \ddot{q}_j(t) + \bar{C}_j \dot{q}_j(t) + \bar{K}_j q_j(t) = \bar{F}_j \tag{A.1}$$

where $\bar{M}_j$ the generalized mass and calculated as

$$\bar{M}_j = \int_0^l \phi_j(x)\, \phi_k(x) m(x) dx \tag{A.2}$$

$\bar{C}_j$ the generalized viscous damping and calculated as

$$\bar{C}_j = \int_0^l \phi_j(x)\, \phi_k(x) c(x) dx \tag{A.3}$$

$\bar{K}_j$ the generalized stiffness and calculated as

$$\bar{K}_j = \omega_j^2 \bar{M}_j \tag{A.4}$$

$\bar{F}_j$ the generalized force and calculated as

$$\bar{F}_j = \int_0^l \phi_j(x)\, f(x,t) dx \tag{A.5}$$

and ω_j is modal frequency and $f(x,t) = W \sin \omega t$.

In order to solve (4) there is a need in calculating mode shape and generalized coordinate, which is elaborated as follows. Firstly, by taking into consideration the modal solution the mode shape $\phi_j(x)$ from (2) need to be identified as (Barnoski, 1965)

$$\phi_j(x) = C \cos \lambda_j + D \sin \lambda_j + E \cosh \lambda_j x + F \sinh \lambda_j x \tag{A.6}$$

where C, D, E, F are constants which can be identified from boundary conditions, λ is an argument of beam characteristic equation. The boundary conditions for the current pinned-pinned beam are as follows:

$$\begin{aligned} &\text{for } x = 0; \qquad x(0,t) = 0;\ EI \frac{\partial^2 z(0,t)}{\partial x^2} = 0; \\ &\text{for } x = l; \qquad z(l,t) = 0;\ EI \frac{\partial^2 z(l,t)}{\partial x^2} = 0, \end{aligned} \tag{A.7}$$

which means that deflection and the moment at the beam ends are equal to zero. By applying boundary conditions (A.7) into (A.6) we obtain the mode shapes as (Barnoski, 1965)

$$\phi_j = \sqrt{2}\sin\lambda_j x = \sqrt{2}\sin\frac{j\pi x}{l} \tag{A.8}$$

where l is length of the beam. The multiplication of the amplitude of mode shapes to $\sqrt{2}$ is done for simplicity in solving the generalized mass (Barnoski, 1965). The resonant frequencies can be written as

$$\left(\lambda_j l\right)^4 = \frac{ml^4}{EI}\omega_j^2 \tag{A.9}$$

where $\lambda_j l = j\pi$, for $j = 1,2,\ldots$. Secondly, the generalized coordinate $q_j(t)$ can be found from the following equation (Barnoski, 1965)

$$\ddot{q}_j(t) + 2\zeta_j\omega_j\dot{q}_j(t) + \omega_j^2 q_j(t) = \frac{\bar{F}_j}{\bar{M}_j} \tag{A.10}$$

where ζ_j is damping ratio. The equation (A.10) is second order linear differential equation with constants, which can be solved as (Barnoski, 1965)

$$q_j(t) = \frac{1}{\omega_j^2 - \omega^2 + i2\zeta_j\omega_j\omega}\cdot\frac{\bar{F}_j(x)}{\bar{M}_j} \tag{A.11}$$

or in absolute magnitude form as

$$\left|q_j(t)\right| = \frac{1}{\omega_j^2\sqrt{\left[\left(1-\frac{\omega^2}{\omega_j^2}\right)^2 + \left(2\zeta_j\frac{\omega}{\omega_j}\right)^2\right]}}\cdot\frac{\bar{F}_j(x)}{\bar{M}_j} \tag{A.12}$$

Now by substituting (A.8) into (A.2) we obtain generalized mass as (Barnoski, 1965)

$$\bar{M}_j = 2m\int_0^l \sin\lambda_j \sin\lambda_k\, dx = \begin{cases} ml, & j = k \\ 0, & j \neq k \end{cases} \tag{A.13}$$

and by substituting (A.8) into (A.5) the generalized force can be calculated as (Barnoski, 1965)

$$\bar{F}_j = W\sqrt{2}\int_a^b \sin\lambda_j\, x \sin\omega t\, dx = \frac{2\sqrt{2}W}{\lambda_j}\left(\sin(b+a)\frac{\lambda_j}{2}\cdot\sin(b-a)\frac{\lambda_j}{2}\right)\sin\omega t \quad \text{(A.14)}$$

After calculating generalized mass and force (A.13) and (A.14) can be substituted into (A.11) and (A.12) in order to find the generalized coordinate (Barnoski, 1965).

$$q_j(t) = \frac{1}{\omega_j^2 - \omega^2 + i2\zeta_j\omega_j\omega}\cdot\left(\frac{2\sqrt{2}W}{\lambda_j ml}\left(\sin(b+a)\frac{\lambda_j}{2}\cdot\sin(b-a)\frac{\lambda_j}{2}\right)\sin\omega t\right) \quad \text{(A.15)}$$

Furthermore, the generalized coordinate from (A.15) and the mode shape from (A.8) can be placed into (2), thus the lateral displacement of pinned-pinned beam excited by uniform loading distributed over a partial length can be in general form written as (Barnoski, 1965):

$$z(x,t) = \frac{4W}{ml}\sum_j^{\infty}\frac{\sin\lambda_j x}{\lambda_j\left(\omega_j^2 - \omega^2 + i2\zeta_j\omega_j\omega\right)} \cdot\left(\left(\sin(b+a)\frac{\lambda_j}{2}\cdot\sin(b-a)\frac{\lambda_j}{2}\right)\sin\omega t\right) \quad \text{(A.16)}$$

and the absolute magnitude can be written as

$$|z(x)| = \frac{4W}{ml}\sum_j^{\infty}\frac{\sin\lambda_j x}{\lambda_j\left(\omega_j^2\sqrt{\left[\left(1-\frac{\omega^2}{\omega_j^2}\right)^2 + \left(2\zeta_j\frac{\omega}{\omega_j}\right)^2\right]}\right)} \cdot\left(\left(\sin(b+a)\frac{\lambda_j}{2}\cdot\sin(b-a)\frac{\lambda_j}{2}\right)\sin\omega t\right) \quad \text{(A.17)}$$